

# Wettability Conversion of an Aluminum-hydroxide Nanostructure by Ion Implantation

Jihoon JEON and Dukhyun CHOI\*

*Department of Mechanical Engineering, Kyung Hee University, Yongin 17104, Korea*

Hyungdae KIM

*Department of Nuclear Engineering, Kyung Hee University, Yongin 17104, Korea*

Yong Tae PARK

*Department of Mechanical Engineering, Myongji University, Youngin 17058, Korea*

Min-Jun CHOI and Kwun-Bum CHUNG†

*Division of Physics and Semiconductor Science, Dongguk University, Seoul 04620, Korea*

(Received 4 March 2016, in final form 21 March 2016)

This work presents a method for controlling the wettability of an aluminum-hydroxide ( $\text{Al}(\text{OH})_3$ ) nanostructure by using ion implantation. We implant Xe ions into  $\text{Al}(\text{OH})_3$  nanostructures at dosages between  $5 \times 10^{14}$  to  $1 \times 10^{16}$  ions/cm<sup>2</sup>. The microscopic surface morphology of the nanostructure after implantation does not change under our dosing conditions. However, a drastic increase in the surface contact angle (CA) from 0° to 100° is observed at a dosage of  $5 \times 10^{15}$  ions/cm<sup>2</sup>. We attribute this significant change in CA to the composition and chemical bonding states of carbon contained within the  $\text{Al}(\text{OH})_3$  nanostructure.

PACS numbers: 81.07.-b, 68.47.Gh, 61.72.Ww

Keywords: Aluminum hydroxide, Ion implantation, Xe ions, Contact angle, X-ray photoelectron spectroscopy

DOI: 10.3938/jkps.68.1024

## I. INTRODUCTION

Controlling the wettability of solid surfaces is important in various industrial processes [1–8], including printing, adhesion, and coating. Lithographic approaches [9], micromachining [10], plasma surface treatments [11, 12] and chemical deposition [13] have all been used to make surfaces either hydrophilic or hydrophobic because the wettability of a solid surface is strongly influenced both by its chemical composition and by its geometric structure. Most of these methods, however, are time-consuming processes, requiring costly specialized equipment and elevated temperatures.

Ion implantation is an effective materials engineering process that can be used to change the surface, chemical, or electrical properties of a solid material. Ion implantation is especially useful in cases where a chemical or structural change is desired near the surface of the target material. Controlling the wettability of poly-

mer surfaces by using electron beam implantation has been well studied. Random micropatterning of a polymer surface, created by the irradiation, results in significant changes in the contact angle (CA) [14,15]. Our group recently demonstrated the potential for wettability control of nanoporous oxide materials by ion implantation [16]. Because the surface of the oxide was dense and hard, no significant changes in the surface morphology occurred, however, the CA changed by approximately 40°. We attributed this change to the surface cleaning effect (*i.e.*, surface sputtering).

In this study, we prepared large-area aluminum-hydroxide ( $\text{Al}(\text{OH})_3$ ) nanostructures, by using simple wet chemistry and investigated their wettability after implantation of Xe ions on the surface. The fluence of Xe ions ranged from  $5 \times 10^{14}$  to  $1 \times 10^{16}$  ions/cm<sup>2</sup>. The depth profile of the Xe ions and the energy loss within the  $\text{Al}(\text{OH})_3$  nanostructures were calculated by using The Stopping and Range of Ions in Matter (SRIM) code. The ion-implanted  $\text{Al}(\text{OH})_3$  nanostructures were further characterized using field-emission scanning electron microscopy (FE-SEM) for surface morphology, CA

\*E-mail: dchoi@khu.ac.kr

†E-mail: kbchung@dongguk.edu

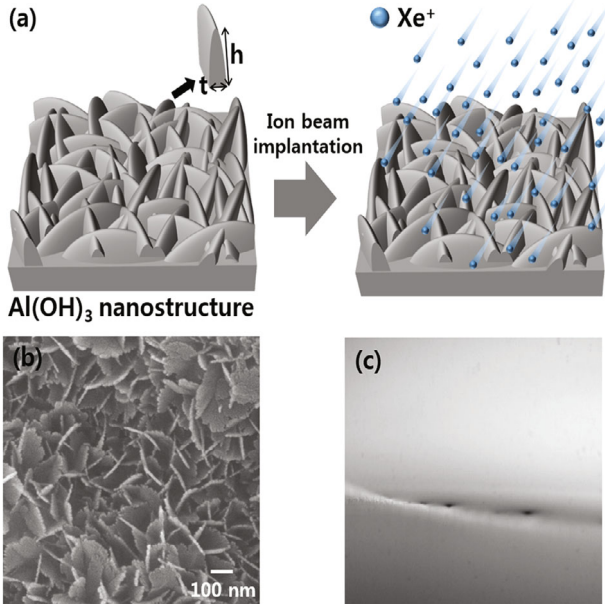


Fig. 1. (Color online) (a) Schematic illustration of ion implantation in an  $\text{Al}(\text{OH})_3$  nanostructure. (b) Top-view FE-SEM image of an  $\text{Al}(\text{OH})_3$  nanostructure. (c) Contact angle (CA) of an as-grown  $\text{Al}(\text{OH})_3$  nanostructure, which is approximately  $0^\circ$  (superhydrophilic character).

measurements for the surface energy, and X-ray photoelectron spectroscopy (XPS) for the composition and the chemical bonding states.

## II. EXPERIMENTS AND DISCUSSION

Figure 1(a) shows a schematic illustration of an ion-implanted  $\text{Al}(\text{OH})_3$  nanostructure. Industrial aluminum (Al) sheets (99.5% purity) were used to synthesize the  $\text{Al}(\text{OH})_3$  nanostructures. The fabrication process is simple and allows for large-area nanostructures, over 5 cm, to be obtained. First, the industrial Al sheet is immersed in a 0.05 M NaOH solution at  $80^\circ\text{C}$  for 10 min after typical cleaning processes. Here, the Al surface naturally oxidizes, forming a thin  $\text{Al}_2\text{O}_3$  layer on its outmost surface. This Al sheet is then placed in boiling deionized water for 10 min. After these steps, a large-area  $\text{Al}(\text{OH})_3$  nanoflake, as shown in the SEM image of Fig. 1(b), is obtained. The nanoflakes are approximately  $20 \sim 30$  nm in the thickness ( $t$ ) and about  $\sim 1 \mu\text{m}$  in height ( $H$ ). We can summarize the chemical reactions from the above processes with the following reactions:

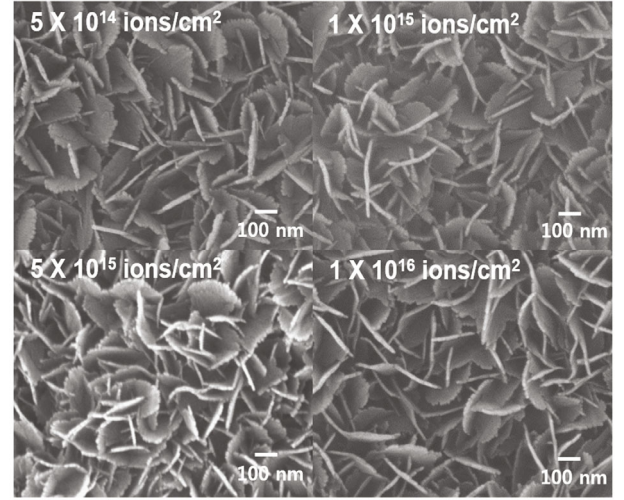
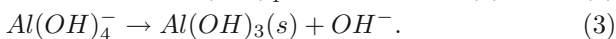
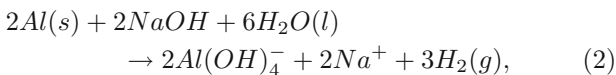
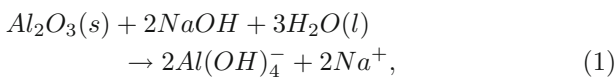


Fig. 2. FE-SEM images of  $\text{Al}(\text{OH})_3$  nanostructure according to Xe ion dose. The Scale bar = 100 nm.

The aluminate ions  $[\text{Al}(\text{OH})_4^-]$  in the gelatinous layer transform into  $\text{Al}(\text{OH})_3$  with a nanoscale microstructure in the boiling water. If the surface is to be stabilized, the specimen must be immersed in boiling water immediately after reacting with the NaOH solution. The as-grown  $\text{Al}(\text{OH})_3$  nanostructures normally provide a superhydrophilic character ( $\text{CA} \sim 0^\circ$ ) due to their geometric and chemical properties, as shown in Fig. 1(c). After the  $\text{Al}(\text{OH})_3$  nanostructures had been prepared, Xe ion implantation was carried out at room temperature with 150 keV protons generated from a 300 keV ion implanter at the Advanced Radiation Technology Institute (ARTI, Republic of Korea). The pressure inside the implanter's target chamber was kept at  $10^{-5}$  Torr. The total fluence varied from  $5 \times 10^{14}$  to  $1 \times 10^{16}$  ions/ $\text{cm}^2$ . The current density of the beam was fixed at less than  $1.0 \mu\text{A}/\text{cm}^2$  to prevent thermal effects on the samples.

Figure 2 shows top-view FE-SEM images of the  $\text{Al}(\text{OH})_3$  nanostructures as a function of the Xe ion dosage. We were unable to find any clear alterations in surface morphology as a result of ion implantation. In our previous report [16], ion implantation was found to potentially lead to a surface sputtering effect. The geometry of the  $\text{Al}(\text{OH})_3$  nanoflakes used presently is greater than several hundreds of nanometers, meaning that the nanoscale details could not be seen in the microscopic images.

Figure 3 shows the simulation results for the projected depth (range), number of atoms, and energy loss calculated using the SRIM code. The simulated structure was comprised of  $\text{Al}(\text{OH})_3$  with an effective thickness of  $1.5 \mu\text{m}$  supported on an Al substrate, and the acceleration energy of the Xe ion was kept at 150 keV. Even though a small number of Xe ions remained inside the  $\text{Al}(\text{OH})_3$  layer, the acceleration energy was deemed adequate for the Xe ions to completely pass through the surface region of the  $\text{Al}(\text{OH})_3$  nanostructure (see Fig. 3(a)). Con-

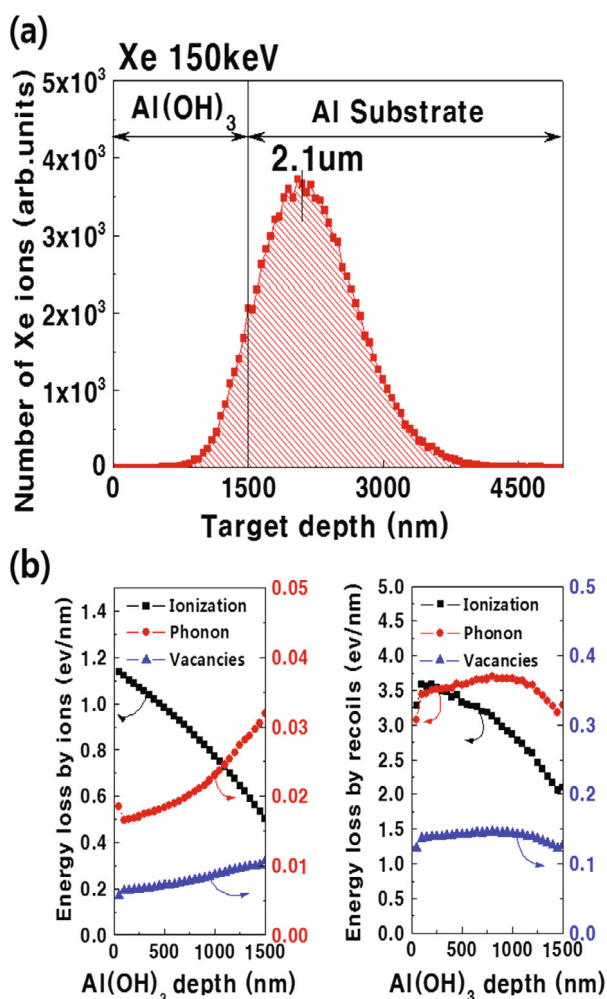


Fig. 3. (Color online) (a) Simulation of the dependence of a Xe ion's trajectory on the penetration depth within  $\text{Al}(\text{OH})_3$  films at an ion acceleration energy of 150 keV. (b) Dependence of the energy loss in the depth direction on the type of energy loss.

sequently, because the Xe ions are not incorporated into the surface region of the  $\text{Al}(\text{OH})_3$  nanostructure, the i effect will not be expected in the surface region. Figure 3(b) shows the energy loss, as a function of depth, depending on the ionization energy, phonon energy, and vacancy energy. Most of the energy loss is generated by the ionization of  $\text{Al}(\text{OH})_3$  in the surface region. This indicates that, due to the ionization bonds caused by the Xe ions, a high potential exists for the formation of new bonds to the  $\text{Al}(\text{OH})_3$  surface.

Figure 4 shows the CA of water applied to the different surfaces as a function of the Xe ion dosage. Interestingly, the CA was found to abruptly change from  $\sim 0^\circ$  to  $120^\circ$  after a dosage of  $5 \times 10^{15}$  ions/cm<sup>2</sup> had been applied. Generally, the CAs of polymer surfaces after ion implantation show such large changes due to the significant changes in the surface morphology [15]. The surfaces of oxides and hydroxides, however, are dense and

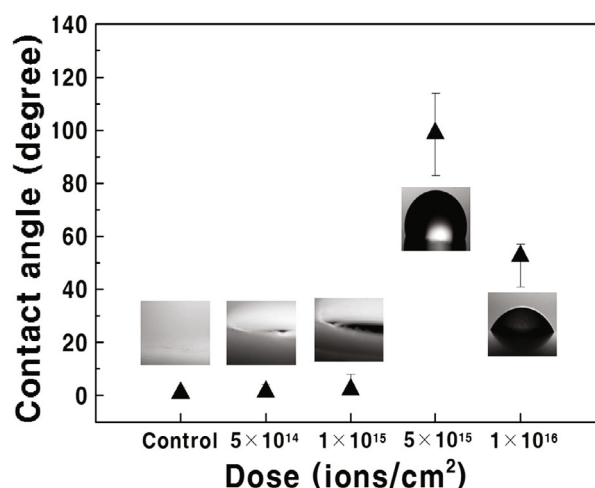


Fig. 4. CA measurements on  $\text{Al}(\text{OH})_3$  nanostructures according to the Xe ion dose. The CAs were measured at ten different positions and averaged; then, standard deviations were calculated.

hard, so they rarely change after ion implantation. Our previous results also showed that the CA change due to the surface sputtering effect is at most  $40^\circ$  [16].

To better understand the CA behavior of  $\text{Al}(\text{OH})_3$  nanostructures after Xe ion implantation, we investigated the chemical composition and bonding states by using XPS. We measured the XPS spectra after eliminating surface contamination from adsorbed OH, C, H<sub>2</sub>O, etc. and minimizing the preferred sputtering of light elements by using Ne ions at 500 eV. Figure 5(a) shows the change in the composition as a function of the Xe ion dosage. We found a high amount of carbon ( $\sim 20\%$ ) in the control sample (*i.e.*, as-grown  $\text{Al}(\text{OH})_3$ ). As mentioned previously,  $\text{Al}(\text{OH})_3$  is an unstable phase, so carbon and oxide are easily incorporated into the surface, creating carbon bonds. The two  $\text{Al}(\text{OH})_3$  nanostructures with superhydrophilic surfaces (made with dosages of  $5 \times 10^{14}$  ions/cm<sup>2</sup> and  $1 \times 10^{15}$  ions/cm<sup>2</sup>) had carbon compositions similar to that of the control sample. The relative carbon composition of the hydrophobic sample, made using a  $5 \times 10^{15}$  ions/cm<sup>2</sup> dosage, increased by approximately two times (*i.e.*,  $\sim 40\%$ ). A further dosage of  $1 \times 10^{16}$  ions/cm<sup>2</sup>, however, once again led to a decrease in the carbon content and a hydrophilic surface. The decrease in the carbon composition at a dosage of  $1 \times 10^{16}$  ions/cm<sup>2</sup> can be explained by using the surface sputtering effect.

The chemical bonding states of the O1s and the C1s spectra were analyzed, and the results are shown in Fig. 5(b) and (c). The O1s spectra were carefully deconvoluted into these peaks (O1, O2, O3) by using a Gaussian fitting by the subtraction of a Shirley-type background and by considering the methods used in a previous report [17]. The low binding-energy peak (O1) at 529.9 eV is related to the O<sup>2-</sup> ions in the metal oxides, indicating either Al-O or Al-OH bonds [18]. The peak at

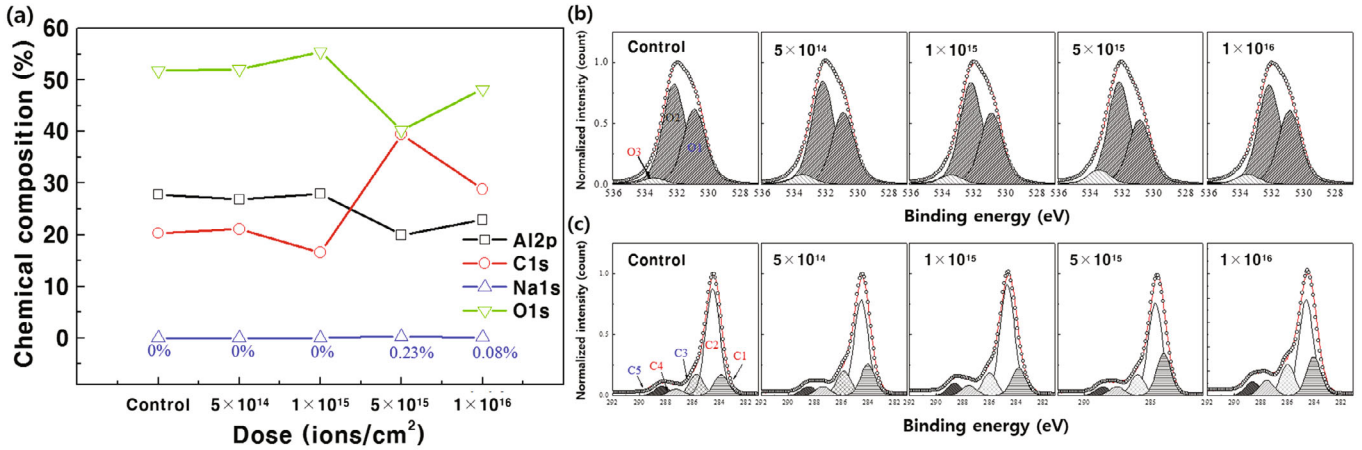


Fig. 5. (Color online) (a) Relative chemical composition of Al(OH)<sub>3</sub> films, (b) O 1s spectra, and (c) C 1s spectra as functions of Xe ion implantation dose. O1, C3, and C5 (blue) represent hydrophilic bonding states, and O3, C1, C2, and C4 (red) represent hydrophobic bonding states, respectively.

the medium binding energy (O2) of the O1s spectrum is associated with OH bonding species and with O<sup>2-</sup> ions that are in the oxygen-deficient Al-O bonding matrix. The higher binding-energy peak (O3) around 532.7 eV is typically attributed to chemisorbed or dissociated oxygen or OH species on the surfaces of the Al(OH)<sub>3</sub> nanostructures. These are typically -CO<sub>3</sub>, adsorbed H<sub>2</sub>O, or adsorbed O<sub>2</sub>. The dominant chemical bonding state of the O3 peak could be interpreted as the carbon-related chemical bonding states due to the minimization of surface contamination before measuring by sputtering. The density of the metal-oxide bonding states (O1), on samples with hydrophilic surfaces, decreases with increasing Xe ion dose until a dosage of 5 × 10<sup>15</sup> ions/cm<sup>2</sup> is reached. It also increases in the Al(OH)<sub>3</sub> nanostructure with a 1 × 10<sup>16</sup> ions/cm<sup>2</sup> dosage. Another interesting finding was how the carbon-related chemical bonding (O3) changed with the hydrophobic properties, similar to the tendencies seen for the relative carbon composition in Fig. 5(a). In order to determine the detailed carbon bonding states, we analyzed the C 1s spectra from Fig. 5(c) and deconvoluted them into five Gaussian peaks (C1, C2, C3, C4, C5). The carbon-bonding peaks refer to double carbon bonds (C=C, C1), to (CH<sub>2</sub>)<sub>n</sub> or C-C bonds (C2), to C-OH bonds (C3), to carbon oxygen double bonds (C=O, C4), and to COOH or COO<sup>-</sup> bonds (C5), respectively [19,20]. Of significance is the decrease in the C3 and the C5 bonding states, which occur concurrently with changes in the hydrophilic properties of the Al(OH)<sub>3</sub> nanostructure at a dosage of 5 × 10<sup>15</sup> ions/cm<sup>2</sup>. This is noteworthy when compared to the Al(OH)<sub>3</sub> nanostructures with relatively hydrophobic surfaces. In addition, the Al(OH)<sub>3</sub> nanostructure, made with a dosage of 5 × 10<sup>15</sup> ions/cm<sup>2</sup>, showed the highest relative ratio of other carbon bonding states (C1, C2, C4); this is characteristic of hydrophobic surfaces.

### III. CONCLUSION

In conclusion, we investigated the wettability conversion of Al(OH)<sub>3</sub> nanostructures due to Xe ion implantation. Based on simulations using the SRIM code, we confirmed that our implantation conditions were effective in irradiating the surface of Al(OH)<sub>3</sub> nanostructures and that the reactivity of the surface was activated due to the high ionization energy loss at the surface. Even though the surface morphology did not change significantly, the CA changed abruptly from 0° to 100° after a Xe ion dose of 5 × 10<sup>15</sup> ions/cm<sup>2</sup> had been applied. From XPS analyses, we determined that the reason for this abrupt change in the CA stemmed from the carbon composition and carbon bonding states (C1, C2, C4) in the nanostructure, which altered the hydrophobic characteristics.

### ACKNOWLEDGMENTS

This work was financially supported by a grant from Kyung Hee University in 2014 (KHU-20140327). This work was also supported by the Fundamental Technology Research Program (NRF-2014M3A7B4052202) and by the framework of international cooperation program (NRF-2015K2A2A7056357) through a National Research Foundation of Korea funded by the Ministry of Science, ICT and Future Planning (MSIP).

### REFERENCES

- [1] H. Irie, T. S. Ping, T. Shibata and K. Hashimoto, *Electrochem. Solid-State Lett.* **8**, D23, (2005).

- [2] R. Wang, K. Hashimoto, A. Fujishima, M. Chikuni, E. Kojima, A. Kitamura, M. Shimohigoshi and T. Watanabe, *Nature* **388**, 431 (1997).
- [3] Y. Zhou, B. Wang, X. Song, E. Li, G. Li, S. Zhao and H. Yan, *Appl. Surf. Sci.* **253**, 2690 (2006).
- [4] X. Zhang, F. Shi, J. Niu, Y. Jiang and Z. Wang, *J. Mater. Chem.* **18**, 621 (2008).
- [5] D. Hegemann, H. Brunner and C. Oehr, *Nucl. Instr. Meth. Phys. Res. B: Beam interact. Mater. atoms* **208**, 281 (2003).
- [6] T. Young, *Philosoph. Trans. Roy. Soc. London* **95**, 65 (1805).
- [7] R. N. Wenzel, *Indust. Engineer. Chem.* **28**, 988 (1936).
- [8] A. Cassie and S. Baxter, *Trans. Faraday Soc.* **40**, 546 (1944).
- [9] B. Liu, Y. He, Y. Fan and X. Wang, *Macromol. Rapid Commun.* **27**, 1859 (2006).
- [10] Z. Yoshimitsu, A. Nakajima, T. Watanabe and K. Hashimoto, *Langmuir* **18**, 5818 (2002).
- [11] J. Lai, B. Sunderland, J. Xue, S. Yan, W. Zhao, M. Folkard, B. D. Michael and Y. Wang, *Appl. Surf. Sci.* **252**, 3375 (2006).
- [12] N. Zhao, F. Shi, Z. Wang and X. Zhang, *Langmuir* **21**, 4713 (2005).
- [13] J. Ou, W. Hu, M. Xue, F. Wang and W. Li, *ACS Appl. Mater. Interfaces* **5**, 3101 (2013).
- [14] S. Yoshiaki, K. Masahiro and I. Masaya, *Nucl. Instr. Meth. Phys. Res. B: Beam Interact. Mater. Atoms* **91**, 584 (1994).
- [15] E. J. Lee, C. Jung, I. Hwang, J. Choi, S. O. Cho and Y. Nho, *ACS Appl. Mater. Interfaces* **3**, 2988 (2011).
- [16] Y. Bae, J. Jeon, C. Jung and D. Choi, *J. Mech. Sci. Tech.* **28**, 3219 (2014).
- [17] B. D. Ahn, J. H. Lim, M. Cho, J. S. Park and K. B. Chung, *J. Phys. D* **45**, 415307 (2012).
- [18] J. A. Rotole and P. M. Sherwood, *J. Vacuum Sci. & Tech. A* **17**, 1091 (1999).
- [19] M. J. Kim, Y. Jeong, S. Sohn, S. Y. Lee, Y. J. Kim, K. Lee, Y. H. Kahng and J. H. Jang, *AIP Adv.* **3**, 012117 (2013).
- [20] N. Vandencastele and F. Reniers, *J. Electron Spect. Related Phenom.* **178**, 394 (2010).